

Sources and losses of energetic protons in Saturn's magnetosphere

C. Paranicas^{a,*}, D.G. Mitchell^a, S.M. Krimigis^a, D.C. Hamilton^b, E. Roussos^c, N. Krupp^c, G.H. Jones^{d,e}, R.E. Johnson^f, J.F. Cooper^g, T.P. Armstrong^h

^a The Johns Hopkins University Applied Physics Laboratory, MS MP3-E128, 11100 Johns Hopkins Rd., Laurel, MD 20723, USA

^b Department of Physics, University of Maryland, College Park, MD 20742, USA

^c Max-Planck-Institut fuer Sonnensystemforschung, 37191 Katlenburg-Lindau, Germany

^d MSSL, University College London, Holmbury St. Mary, Dorking, Surrey RH5 6NT, UK

^e Centre for Planetary Sciences, University College London, Gower Street, London WC1E 6BT, UK

^f University of Virginia, Thornton Hall, Charlottesville, VA 22904, USA

^g Heliospheric Physics Lab, NASA Goddard Space Flight Center, Greenbelt, MD 20771, USA

^h Fundamental Technologies, Lawrence, KS 66046, USA

ARTICLE INFO

Article history:

Received 5 February 2008

Revised 24 April 2008

Available online 4 June 2008

Keywords:

Saturn, magnetosphere

Saturn, satellites

Saturn, rings

Satellites, surfaces

ABSTRACT

We present Cassini data revealing that protons between a few keV and about 100 keV energy are not stably trapped in Saturn's inner magnetosphere. Instead these ions are present only for relatively short times following injections. Injected protons are lost principally because the neutral gas cloud converts these particles to energetic neutral atoms via charge exchange. At higher energies, in the MeV to GeV range, protons are stably trapped between the orbits of the principal moons because the proton cross-section for charge exchange is very small at such energies. These protons likely result from cosmic ray albedo neutron decay (CRAND) and are lost principally to interactions with satellite surfaces and ring particles during magnetospheric radial diffusion. A main result of this work is to show that the dominant energetic proton loss and source processes are a function of proton energy. Surface sputtering by keV ions is revisited based on the reduced ion intensities observed. Relatively speaking, MeV ion and electron weathering is most important closer to Saturn, e.g. at Janus and Mimas, whereas keV ion weathering is most important farther out, at Dione and Rhea.

© 2008 Elsevier Inc. All rights reserved.

1. Introduction

In planetary radiation belts, high fluxes of energetic ions and electrons form persistent distributions close to the planet. There are several sources of energetic charged particles in Saturn's magnetosphere including cosmic ray albedo neutron decay (CRAND) (Fillius and Ip, 1980) and injections. Once in the inner magnetosphere, these energetic particles do not remain trapped indefinitely. There are many loss mechanisms relevant to outer planet magnetospheres including wave-particle scattering into the atmospheric loss cone, absorption by moons and rings, charge-exchange with neutrals, and others. In this paper, we will focus on measured protons in the keV to tens of MeV energy range. Roussos et al. (2007) have previously analyzed the interactions of energetic electrons with the saturnian moons. Our main goals here are to present new proton data, suggest loss and source processes by energy range, and discuss the consequences of these findings for satellite surface weathering.

Data presented in this paper are from Cassini's Magnetospheric Imaging Instrument (MIMI). MIMI has three separate sensors: the charge-energy-mass spectrometer (CHEMS), the low energy magnetospheric measurements system (LEMMS), and the ion and neutral camera (INCA). We present data only from CHEMS and LEMMS here. CHEMS can detect and discriminate among ions in the 3–220 keV/e range. It has the capacity to make triple-coincidence measurements that help to reduce the effects of penetrating background. LEMMS can nominally detect ions in the total energy range from about 30 keV to tens of MeV. A complete description of the instrument can be found in Krimigis et al. (2004).

2. Losses to satellites and rings

In discussing protons trapped in Saturn's inner magnetosphere, we begin with the quasi-stably trapped particles above 1 MeV. In Fig. 1, we show the intensities of 12.1–58.9 MeV protons from the LEMMS sensor. This proton channel does not appear to be affected by penetrating background, potentially more significant in the lower energy LEMMS ion channels. Data were obtained during Saturn Orbit Insertion (SOI) on days 2004-182 to 2004-183. Here we have transformed the data into intensity and binned them by

* Corresponding author. Fax: +1 (240) 228 0386.

E-mail address: chris.paranicas@jhuapl.edu (C. Paranicas).

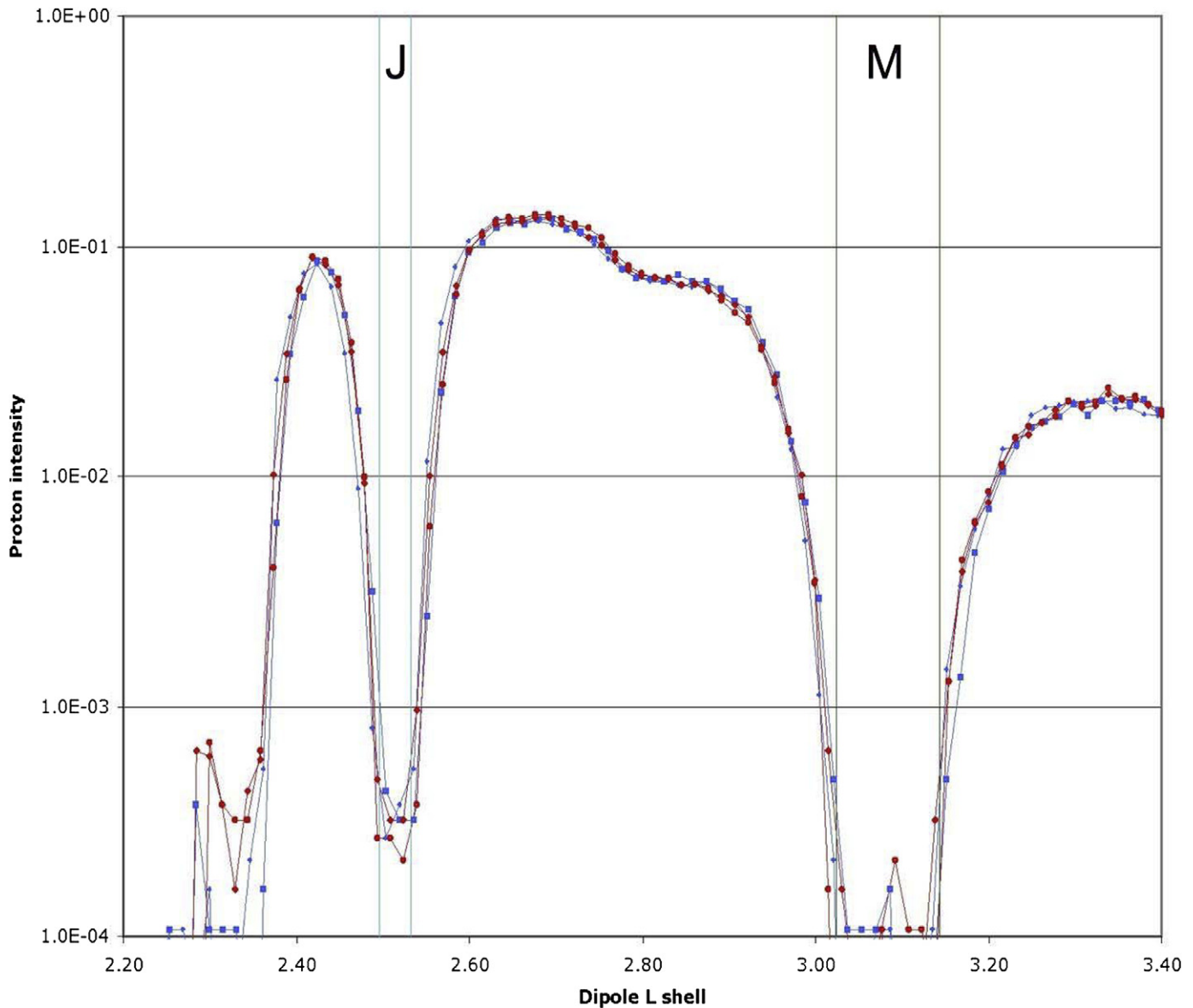


Fig. 1. Proton intensity (protons per $\text{cm}^2 \text{sr keV}$) as a function of L shell during SOL. To compute dipole L shell of the spacecraft and satellites, an offset dipole is used with moment along Saturn's spin axis. We plot (as separate curves) only those points corresponding to equatorial pitch angles of $25\text{--}35^\circ$ and $145\text{--}155^\circ$. Furthermore, we have indicated which points were taken during the inbound (blue) and outbound (red) portion of the trajectory. Positions of the Satellites Janus ($L \sim 2.5$) and Mimas ($L \sim 3.1$) are shown as sweeping corridors.

equatorial pitch angle. The equatorial pitch angles were computed from the local pitch angle using a dipolar magnetic field model. We plot intensities for pitch angles in the ranges $25^\circ\text{--}35^\circ$ (and equivalently $145^\circ\text{--}155^\circ$). Furthermore, we have indicated which points were taken during the inbound (blue) and outbound (red) portion of the trajectory and separately connect the small and large pitch angles with solid lines.

The L shell used in Fig. 1 was calculated for an aligned dipole with its center offset northwards by 2230 km or $0.037 R_S$ (Dougherty et al., 2005). For this work, we use $1 R_S = 60,268$ km. Vertical lines are drawn for the positions of the sweeping corridors of Janus and Mimas. These corridor positions were calculated by first finding the minimum and maximum L shells of the moon centers of mass for the relevant time period. To do this, we used the satellite ephemerides from the SPICE kernel (see <http://naif.jpl.nasa.gov/naif/>) and transformed the satellite positions into the SKR system (Kurth et al., 2007). The moon radius is subtracted from the minimum L value and added to the maximum L to give the plotted sweeping corridor. The proton intensity

decreases in this energy range are well organized by the satellite locations.

These broad absorptions by satellites seen in Fig. 1 are referred to as macrosignatures because they are observed every time a spacecraft crosses a moon's orbit. Satellite macrosignatures detected over an extended time period during the Cassini mission are visible in Fig. 4.7 of Roussos (2008). Earlier detections of these features in Saturn's inner magnetosphere made during the Pioneer 11 and Voyager 2 missions have been reviewed by Van Allen (1984). Finally, macrosignatures at Enceladus's orbit in MeV protons were previously reported by Jones et al. (2006). Here we are highlighting these features to emphasize that MeV protons are impacting the Satellites Janus, Mimas, and Enceladus, and that satellite absorption is the dominant loss process for these protons at MeV energies. As we see below, for protons at keV energies, no such organization of the data by satellite position occurs.

In addition to the actual absorptions by the satellites, it is interesting to consider why proton intensities began to fall off inward to the sweeping corridors from both larger and smaller radial dis-

tances. For 25 MeV protons with equatorial pitch angles of 30° , the gyroradius is 506 km ($0.008 R_S$) near Mimas and 274 km ($0.005 R_S$) near Janus. This means the sweeping corridors plotted in Fig. 1, which should be slightly larger to account for different proton gyroradii, are a good approximation for all proton energies of interest here. Furthermore, the shoulders of the decreases cannot be accounted for as gyroradius effects but are instead due to the effects of radial diffusion in the vicinity of the moon sweeping regions. The timescales for proton loss are shorter near these corridors than at other radial distances between the moon orbits. In a diffusive random walk (e.g. Cheng, 1986), protons moving radially into sweeping regions have little chance of escaping moon encounters and subsequent loss from the radiation belt population. Likewise, the sweeping corridors themselves are so highly depleted of these protons that random walk radial diffusion out of them is a negligible replenishing source of these protons on neighboring L shells.

In addition to the losses due to the satellites themselves, there is also a small decrease at the F ring ($R \sim 2.33 R_S$), and an inflection at the G ring ($R \sim 2.82 R_S$). These magnetospheric CRAND protons do not penetrate into the main rings. Due to limited knowledge about the G-ring size distribution, the loss processes in this ring are not completely understood, but the G-ring absorption feature does appear for all protons at CRAND energies, as previously measured by Pioneer 11 and Voyager 2. That is, the presence of this feature in a radial intensity profile indicates a dominant response of the detector channel to such protons and not to low energy protons or to electrons. The stopping distance of 10 MeV protons in ice is about 1 mm. If the size distribution of G ring grains (see, for example, Showalter and Cuzzi, 1993) is heavily weighted toward smaller particles, then it would take the cumulative effect of many collisions to slow the protons in questions. On the other hand, Hedman et al. (2007) have reported a concentrated arc of material at a Saturn distance of about 167,500 km (or about $2.78 R_S$) that may be more efficient at slowing and/or stopping MeV protons than a more diffuse population of grains. We do not know if the MeV protons are progressively slowed out of the energy passband (here 12.1–58.9 MeV) by successive collisions with very small grains or are quickly stopped by a collision with a component of the arc. In any case, the organization of the proton data by the moons and rings, with both inbound and outbound in good agreement, reveals that these are the main absorbers of MeV protons.

3. Charge-exchange losses

In addition to satellites and rings, Saturn is unique because of the dense cloud of cold neutrals surrounding it. Both in situ and remote observations have confirmed the presence of significant distributions of neutral atoms and molecules in Saturn's inner magnetosphere (e.g. Shemansky and Hall, 1992). Radial profiles of neutral densities consistent with observation and modeling were developed prior to Cassini's arrival at the planet (see summary in Richardson, 1998; Jurac and Richardson, 2005). The profiles of H, OH, H_2O , and O peak near the orbit of the Satellite Enceladus, $R = 3.95 R_S$. In the Jurac and Richardson (2005) model, which is self-consistent with the Voyager plasma ion data (Richardson and Jurac, 2004), the water profile falls off by more than an order of magnitude between Enceladus's orbit and Rhea's at $R = 8.74 R_S$. Hydrogen atoms form the most extended distribution because the energy of dissociation of water and OH molecules imparts a higher random, thermal velocity to the light hydrogen fraction than to the heavier OH or oxygen component. Although the neutral source has been shown to occur at the orbit of Enceladus (Jurac et al., 2002), the nature of the neutral source was not explained prior to Cassini's close flybys of the Satellite Enceladus. Data from those

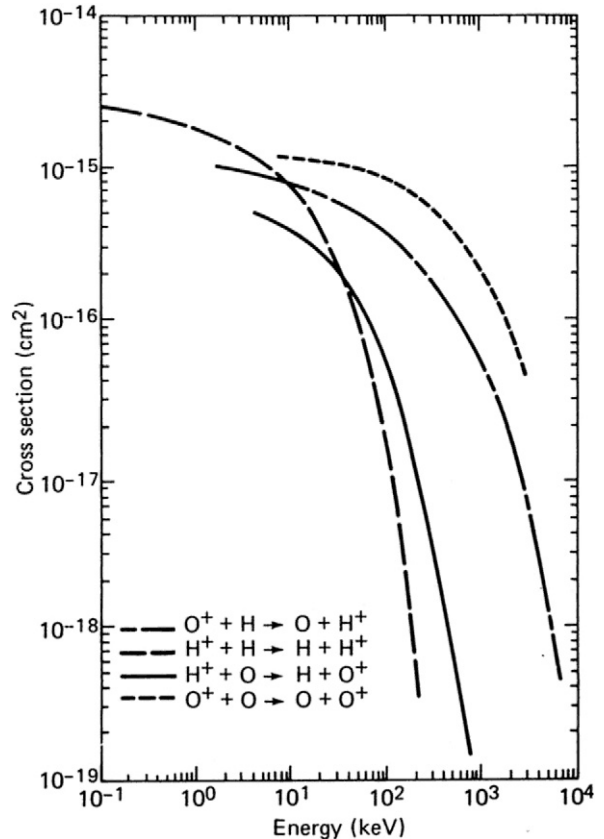


Fig. 2. Charge-exchange cross-sections for protons and singly charged oxygen on neutral H and O. From McEntire and Mitchell (1989). Reproduced by permission of American Geophysical Union. Copyright 1989 American Geophysical Union.

passes revealed a south polar plume of water vapor and dust (Hansen et al., 2006; Porco et al., 2006) that populates the cloud. Johnson et al. (2006) used modeling of plume emissions to show the connection between the plumes and the extended neutral torus. They further showed that there exists a very narrow, higher density torus at Enceladus's orbit.

Ions (both thermal plasma and in the higher energy part of the distribution) can undergo charge exchange (CE) with components of the cold gas cloud. In these collisions, a singly-charged ion becomes an energetic neutral atom (ENA) while retaining almost all of its initial energy. In Fig. 2, we show a compilation of CE cross-sections of protons and O^+ on neutral hydrogen and oxygen from McEntire and Mitchell (1989). A similar falloff with energy is seen for protons on water (see Fig. 2.3 of Johnson, 1990). Because CE cross-sections for protons on the major neutrals at Saturn begin to drop quickly in the tens of keV range, the MeV protons discussed above are relatively unaffected by the presence of the neutrals. At the other end of the energy spectrum, the thermal plasma mentioned above, appear to be present in high numbers. Fig. 1B of Young et al. (2005) shows a peak intensity associated with very cold protons essentially corotating with the planet; protons at slightly higher and slightly lower energies are much less abundant. These plasma protons do undergo CE collisions with the neutrals, but for each ion lost to CE, a new cold ion is created and picked up in the corotation electric field. Thus, there is no net loss of cold ions in these collisions.

It is the protons above the corotating energy and below a few hundred keV that are strongly affected by charge exchange and we turn to these next. In Figs. 3 and 4, we present spectrograms showing proton intensities detected by the CHEMS sensor. Proton

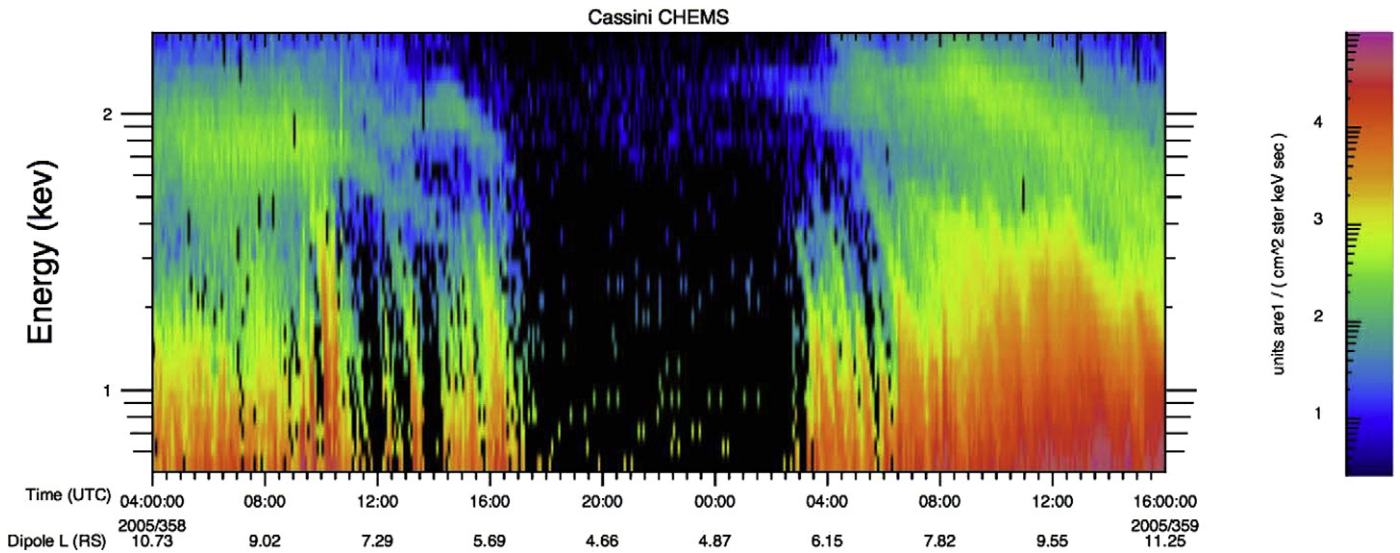


Fig. 3. Proton intensity as a function of time and energy from 2005-358 04:00 to 2005-359 16:00 UTC. These CHEMS data are averaged into 5 min bins and count rate is converted to intensity; only energies between 5 and 200 keV are plotted. Also plotted on the horizontal axis is the dipole L shell of Cassini. During the displayed time period, the spacecraft is within 1° of the spin equator and moves from about local noon past local midnight.

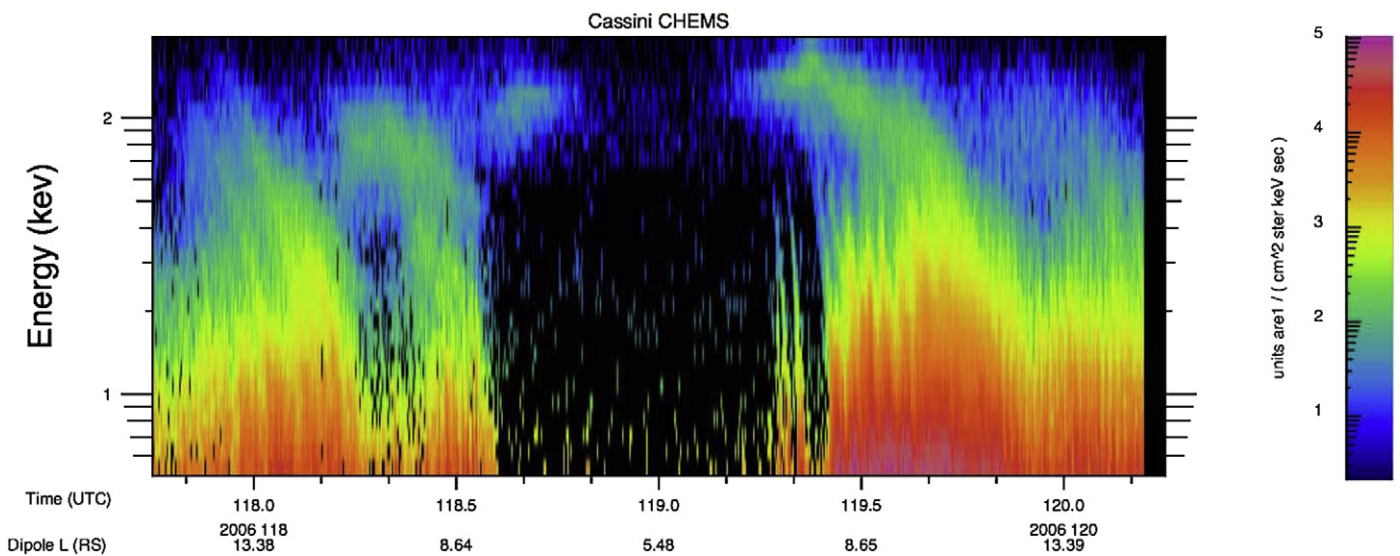


Fig. 4. Same display type as Fig. 3 for data from 2006-117 18:00 to 2006-120 06:00 UTC. For the time displayed, Cassini is within about 1° of the spin equator and moves in local time from morning through noon and dusk.

intensity is plotted as a function of time and energy for two different time periods. Many ion injections (vertical features or features sloping to the left at high energies) can be observed, see discussion below. These figures also reveal high proton intensities that drop off toward the inner magnetosphere. To show the decrease as a function of L shell, we have summed the count rates over the whole CHEMS energy range. In Fig. 5, we display the summed count rates for protons and oxygen ions corresponding to the time intervals in Figs. 3 and 4. The shape of the flux drop off inward to the planet has different behavior on each orbit we have surveyed and is not related to the locations of the moons. If the spacecraft gets close enough to Saturn, the drop off is always present in the data. The black color in Figs. 3 and 4 is the background level of CHEMS and corresponds to an upper limit on the flux in those regions of about one proton per $\text{cm}^2 \text{sr keV}$.

Based on Fig. 2, it is reasonable to conclude that these protons are being lost to CE in the gas cloud. This conclusion is reinforced by our ENA observations (e.g. Paranicas et al., 2005). Recently created ENAs are measured directly by INCA and based on many im-

ages we have been able to locate a primary ENA source at the edge of the densest part of the gas cloud (Carbary et al., 2008).

4. Sources of energetic protons

In this section, we consider the sources of energetic protons, beginning with those in the MeV energy range. If we assume the source of the MeV protons shown in Fig. 1 are all at large distances with inward diffusion and energization, protons have to cross the moon sweeping corridors without being absorbed. The azimuthal speed of ions, or more correctly their guiding centers, is in the same direction as and faster than corotation, so ions always overtake the moons in their orbits. Therefore, unlike with electrons, which can pass radially through sweeping corridors via relatively slow diffusion processes if their azimuthal speed (corotation plus combined gradient and curvature drift) matches the moon's, protons cannot escape absorption in this manner. Therefore the source of these protons cannot be inward diffusion from large distances.

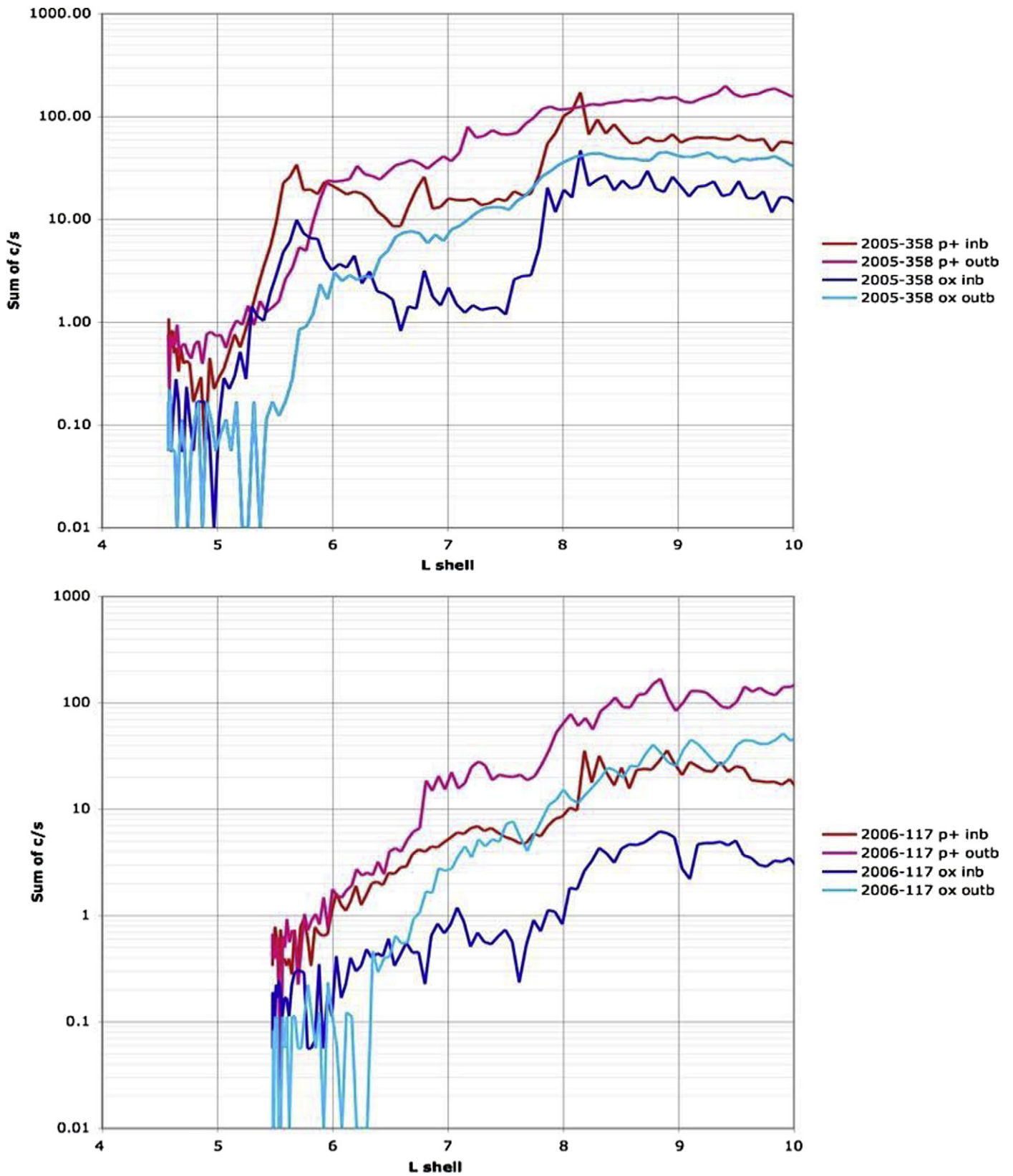


Fig. 5. Summed count rates for the periods in Fig. 3 (top) and Fig. 4 (bottom). The inbound and outbound data are plotted separately with the proton sum red and the oxygen sum blue. The proton (oxygen) sum is over the CHEMS energy range 3–220 (8–220) keV.

Cooper (1983) has modeled radial profiles of these isolated radiation belts using a CRAND source process. In his model, CRAND acts in conjunction with magnetospheric radial diffusion for the injected neutron-decay protons. The injected protons are rapidly lost in the moon sweeping corridors but have diffusive lifetimes of many years in the radial space between these corridors. Additionally in Cooper's work, the diffuse G-ring has a more subtle but distinctive absorption effect on the CRAND proton belts as mentioned above.

While CRAND is likely the source of MeV protons, the protons in the keV range are due to injection activity. Depending on their radial distance and energy, injected protons survive for different lengths of time. Protons lost near the periphery of the main cloud appear to be powering the ENA observations from the inner magnetosphere. Proton injections deeper into the cloud (into the highest density of neutrals) of course have the shortest lifetimes. But protons above about 100 keV can persist for longer times at all distances because of their smaller CE cross-sections.

Next we discuss the various injection features in Figs. 3 and 4 in more detail. For our purposes here, by injections we mean the observational feature of a spatially distinct population of energized protons that appear as close to Saturn as $L \sim 5$. These may be due to flux tube interchange or some other physical mechanism, but here we are only concerned about what we can observe about these features. Injections on these time–energy spectrograms appear as vertical features when they are new and develop time-dispersed shapes as they age (e.g. Mauk et al., 2005). In this type of plot, new ion injections typically curve toward the left with increasing energy because the most energetic ions gradient-curvature drift the fastest and this component of the injection reaches the spacecraft first. We previously demonstrated in our modeling that as injections age, bands in time–energy spectrograms can become horizontal (Paranicas et al., 2007). For example, the nearly horizontal distributions near the tops of Figs. 3 and 4 are likely old injections. The isolated ~ 100 keV proton feature at about 2006-118 16:00 that slopes upward to the right with energy is not as easy to explain. This feature could be the upper energy remnant of an old injection—the lower part lost to CE. However, our modeling also suggests that ion injections older than a couple of days can have rightward curving features. We plan to study these unusual isolated features in later work. To summarize, by performing modeling, we have understood the features in Figs. 3 and 4 as showing a mixture of young and older injections superimposed and there is little doubt now about the source of these trapped populations. Furthermore, it is unusual to find a nearly horizontal (i.e. aged) proton injection below about 100 keV in the densest part of the gas cloud because at low energies the CE cross-sections are very high and the protons do not survive long enough to develop that shape.

5. Implications for moon weathering

Based on the very low fluxes of keV ions discussed above, we next turn to the subject of sputtering. In Jurac et al. (2001a), we transformed Voyager 2 total ion count rates measured near Enceladus to intensities assuming all the ions were oxygen. We did not have the ability to discriminate among ion species below 100 keV, a capability that CHEMS provides on Cassini. At 100 keV, we obtained an intensity of between 10^3 and 10^4 oxygen ions per $\text{cm}^2 \text{sr keV}$. Combined with the lower energy ion data, we estimated a global Enceladus sputtering rate of 10^{25} $\text{H}_2\text{O/s}$. By comparison, we found during Cassini SOI, when the spacecraft crossed Enceladus's orbital distance twice, the intensity upper limit for 100 keV O^+ at that distance is 1 particle per $\text{cm}^2 \text{sr keV}$. In the next section, we discuss this discrepancy further.

Our previous sputtering-based estimates were already shown to be insufficient to create enough neutral gas to support the neutral torus (see Jurac et al., 2001b). As the upper limit on oxygen we have now established with CHEMS is well below what was used previously, this further reduces the importance of sputtering in populating the cloud. But providing an exact revision of the Enceladus sputtering rate is not possible with the CHEMS data only because it does not detect O^+ above a few hundred keV and the peak yield for O^+ on water ice occurs at 2.5 MeV (Johnson, 1990). Based on the CE cross-sections for protons and oxygen shown in Fig. 2 and data presented here, we can conclude that previous calculations of the sputtering yield for the icy saturnian satellites and E-ring grains are not supported by the Cassini data.

Although the previous estimates of the sputtering rates must be re-evaluated, MeV electrons (not discussed here) and ions are present in the inner magnetosphere. For example, Fig. 1 shows the presence of MeV protons well inward of Enceladus's orbit. These particles deposit their energy at depth into the moons and ring particles, chemically altering and decomposing these surfaces. This surface irradiation leads to the production of volatiles such as O_2 and H_2 that have been detected in ionic forms by the Cassini Plasma Spectrometer (CAPS) experiment (Young et al., 2005). Cooper et al. (2006) show that radiolytic chemistry induced by energetic electron bombardment of surface water ice is important on Enceladus. Radiolytic processing rates at other moons scale with electron energy flux, relatively higher at Mimas and lower beyond the orbit of Enceladus (Garrett et al., 2005; Cooper et al., 2006).

As in the Cooper et al. (2006) study then, Mimas and Rhea provide interesting comparison points with regard to a number of weathering phenomena. Data suggest Mimas is heavily weathered by MeV protons but by very few keV range protons. The absence of <200 keV protons is illustrated only inward to about $4.6 R_S$ in this paper, but on other Cassini orbits, this depletion is found to well inward of Mimas's orbit. Rhea is intermittently weathered by keV range protons and, based on Cassini data much lower fluxes of MeV protons (not shown). These two comparison points can be used to study laboratory predictions of the effects of energetic ions on ice (e.g. Loeffler et al., 2006). Finally, a recent compilation of laboratory data for ions of energy below ~ 50 keV has been used along with CAPS ion data to estimate a lower bound to the satellite sputtering rates assuming an absence of energetic heavy ions (Johnson et al., 2008).

6. Discussion

This paper has shown that MeV protons are a robust population in the inner magnetosphere of Saturn. During Cassini SOI, radial intensity profiles of these high energy protons from CRAND do not reveal any azimuthal asymmetry and are well organized by a dipole field model. Distributions are strongly organized by the locations of the planetary moons and rings. Fillius and McIlwain (1980) first suggested the source of MeV protons detected by Pioneer 11 is CRAND from cosmic ray irradiation of Saturn's rings as later quantitatively modeled by Cooper (1983). The Cassini MeV proton measurements close to Saturn are consistent with that conclusion. Further modeling is needed to determine whether radial diffusion alone with known losses and sources can reproduce the exact shape of the data.

In the few keV to hundreds of keV energy range, transient injections appear to be the main source of protons into the inner magnetosphere. Spectrograms show flux patterns that have previously been analyzed as injections of various ages. Loss of these particles is consistent with charge exchange with atoms and molecules in Saturn's giant neutral gas cloud. This results in decreasing proton intensities with decreasing L , reaching the CHEMS sensor back-

ground at $L \sim 5$. We have also put upper limits on the fluxes of energetic O^+ that are well below the Voyager inferred values.

There are two alternative explanations for the discrepancy between the Voyager era keV proton numbers and those we are reporting here. The first is that the nature of the gas cloud was much different during the Voyager encounters. This, however, is not indicated in Cassini measurements of the gas cloud (Esposito et al., 2005), which appear to be consistent with Voyager-based estimates (Richardson, 1998). The second is that the Voyager particle sensors did not have sufficient capacity to differentiate between penetrating background and foreground ion measurements, yielding ion flux measurements that were erroneously high.

In either case, we have shown in the Cassini epoch, Mimas and Enceladus are shielded from the fluxes of keV to ~ 100 keV protons by the extended neutral cloud at Saturn. The surfaces of the innermost moons may still be significantly altered by MeV protons and electrons. The other icy moons outward of Enceladus receive intermittent fluxes of few keV to 100 keV protons, as regulated by the balance among injection intensity and frequency and charge-exchange losses. We have attempted to establish here that the proton losses and sources in Saturn's inner magnetosphere are dominated by different processes at different energies.

Acknowledgments

We appreciate the help of M. Hedman. G.H.J. acknowledges the support of the Science and Technology Facilities Council, UK. This work was partly supported by grants between NASA and JHU/APL. JFC is partly supported by the Cassini Plasma Spectrometer project at NASA Goddard through NASA Jet Propulsion Laboratory contract 1243218 with the Southwest Research Institute in San Antonio.

References

- Carbary, J.F., Mitchell, D.G., Brandt, P., Roelof, E.C., Krimigis, S.M., 2008. Track analysis of energetic neutral atom blobs at Saturn. *J. Geophys. Res.* 113, doi:10.1029/2007JA012708. A01209.
- Cheng, A.F., 1986. Radial diffusion and ion partitioning in the Io torus. *Geophys. Res. Lett.* 13, 517–520.
- Cooper, J.F., 1983. Nuclear cascades in Saturn's rings: Cosmic ray albedo neutron decay and origins of trapped protons in the inner magnetosphere. *J. Geophys. Res.* 88, 3945–3954.
- Cooper, J.F., Sittler Jr., E.C., Cooper, P.D., Burger, M.H., Sturmer, S.J., Rymer, A.M., Hill, M.E., Johnson, R.E., 2006. Energy source contributions from magnetospheric and cosmic ray particle irradiation for the polar plumes of Enceladus. *Bull. Am. Astron. Soc.* 38, 509. Abstract 38.15.06.
- Dougherty, M.K., and 17 colleagues, 2005. Cassini magnetometer observations during Saturn orbit insertion. *Science* 307, 1266–1270.
- Esposito, L.W., and 15 colleagues, 2005. Ultraviolet imaging spectroscopy shows an active saturnian system. *Science* 307, 1251–1255.
- Fillius, W., Ip, W.H., 1980. Trapped radiation belts of Saturn – First look. *Science* 207, 425–431.
- Fillius, W., McIlwain, C., 1980. Very energetic protons in Saturn's radiation belts. *J. Geophys. Res.* 85, 5803–5811.
- Garrett, H.G., Ratliff, J.M., Evans, R.W., 2005. Saturn radiation (SATRAD) model. JPL Pub. 05-09, NASA Jet Propulsion Laboratory.
- Hansen, C.J., Esposito, L., Stewart, A.I.F., Colwell, J., Hendrix, A., Pryor, W., Shemansky, D., West, R., 2006. Enceladus' water vapor plume. *Science* 311, 1422–1425.
- Hedman, M.M., Burns, J.A., Tiscareno, M.S., Porco, C.C., Jones, G.H., Roussos, E., Krupp, N., Paranicas, C., Kempf, S., 2007. The source for Saturn's G ring. *Science* 317, 653–656.
- Johnson, R.E., 1990. *Energetic Charged Particle Interactions with Atmospheres and Surfaces*. Springer-Verlag, Berlin.
- Johnson, R.E., Smith, H.T., Tucker, O.J., Liu, M., Burger, M.H., Sittler, E.C., Tokar, R.L., 2006. The Enceladus and OH tori at Saturn. *Astrophys. J.* 644, L137–L139.
- Johnson, R.E., Famá, M., Liu, M., Baragiola, R.A., Sittler, E.C., Smith, H.T., 2008. Sputtering of ice grains and icy satellites in Saturn's inner magnetosphere. *Planet. Space Sci.*, doi:10.1016/j.pss.2008.04.003, in press.
- Jones, G.H., Roussos, E., Krupp, N., Paranicas, C., Woch, J., Lagg, A., Mitchell, D.G., Krimigis, S.M., Dougherty, M.K., 2006. Enceladus' varying imprint on the magnetosphere of Saturn. *Science* 311, 1412–1415.
- Jurac, S., Johnson, R.E., Richardson, J.D., Paranicas, C., 2001a. Satellite sputtering in Saturn's magnetosphere. *Planet. Space Sci.* 49, 319–326.
- Jurac, S., Johnson, R.E., Richardson, J.D., 2001b. Saturn's E ring and production of the neutral torus. *Icarus* 149, 384–396.
- Jurac, S., McGrath, M.A., Johnson, R.E., Richardson, J.D., Vasyliūnas, V.M., Eviatar, A., 2002. Saturn: Search for a missing water source. *Geophys. Res. Lett.* 29, doi:10.1029/2002GL015855.
- Jurac, S., Richardson, J.D., 2005. A self-consistent model of plasma and neutrals at Saturn: Neutral cloud morphology. *J. Geophys. Res.* 110, doi:10.1029/2004JA010635.
- Krimigis, S.M., and 24 colleagues, 2004. Magnetosphere imaging instrument (MIMI) on the Cassini mission to Saturn/Titan. *Space Sci. Rev.* 114, 233–329.
- Kurth, W.S., Lecacheux, A., Averkamp, T.F., Groene, J.B., Gurnett, D.A., 2007. A saturnian longitude system based on variable kilometeric radiation period. *Geophys. Res. Lett.* 34, doi:10.1029/2006GL028336. L02201.
- Loeffler, M.J., Raut, U., Vidal, R.A., Baragiola, R.A., Carlson, R.W., 2006. Synthesis of hydrogen peroxide in water ice by ion irradiation. *Icarus* 180, 265–273.
- Mauk, B.H., and 11 colleagues, 2005. Energetic particle injections in Saturn's magnetosphere. *Geophys. Res. Lett.* 32, doi:10.1029/2005GL022485.
- McEntire, R.W., Mitchell, D.G., 1989. Instrumentation for global magnetospheric imaging via energetic neutral atoms. In: Waite Jr., J.H., Burch, J.L., Moore, R.L. (Eds.), *Solar System Plasma Physics*. In: *Geophysical Monographs*, vol. 54. AGU, Washington, DC, pp. 69–80.
- Paranicas, C., Mitchell, D.G., Roelof, E.C., Brandt, P.C., Williams, D.J., Krimigis, S.M., Mauk, B.H., 2005. Periodic intensity variations in global ENA images of Saturn. *Geophys. Res. Lett.* 32, doi:10.1029/2005GL023656.
- Paranicas, C., Mitchell, D.G., Roelof, E.C., Mauk, B.H., Krimigis, S.M., Brandt, P.C., Kusterer, M., Turner, F.S., Vandegriff, J., Krupp, N., 2007. Energetic electrons injected into Saturn's neutral gas cloud. *Geophys. Res. Lett.* 34, doi:10.1029/2006GL028676.
- Porco, C.C., and 24 colleagues, 2006. Cassini observes the active south pole of Enceladus. *Science* 311, 1393–1401.
- Richardson, J.D., 1998. Thermal plasma and neutral gas in Saturn's magnetosphere. *Rev. Geophys.* 36, 501–524.
- Richardson, J.D., Jurac, S., 2004. A self-consistent model of plasma and neutrals at Saturn: The ion tori. *Geophys. Res. Lett.* 31. GLO20959.
- Roussos, E., 2008. Interactions of weakly or non-magnetized bodies with Solar System plasmas: Mars and the moons of Saturn. PhD thesis.
- Roussos, E., Jones, G.H., Krupp, N., Paranicas, C., Mitchell, D.G., Lagg, A., Woch, J., Motschmann, U., Krimigis, S.M., Dougherty, M.K., 2007. Electron microdiffusion in the saturnian radiation belts: Cassini MIMI/LEMMS observations of energetic electron absorption by the icy moons. *J. Geophys. Res.* 112, doi:10.1029/2006JA012027. A06214.
- Shemansky, D.E., Hall, D.T., 1992. The distribution of atomic hydrogen in the magnetosphere of Saturn. *J. Geophys. Res.* 97, 4143–4161.
- Showalter, M.R., Cuzzi, J.N., 1993. Seeing ghosts: Photometry at Saturn's G ring. *Icarus* 103, 124–143.
- Van Allen, J.A., 1984. Energetic particles in the inner magnetosphere of Saturn. In: Gehrels, T., Matthews, M.S. (Eds.), *Saturn*. University of Arizona Press, Tucson, pp. 281–317.
- Young, D.T., and 42 colleagues, 2005. Composition and dynamics of plasma in Saturn's magnetosphere. *Science* 307, 1262–1266.